



Persistent Malfunction of Glymphatic and Meningeal Lymphatic Drainage in a Mouse Model of Subarachnoid Hemorrhage

Tinglin Pu¹, Wenyan Zou¹, Weixi Feng¹, Yanli Zhang¹,
Linmei Wang¹, Hongxing Wang^{2*} and Ming Xiao^{1*}

¹Jiangsu Key Laboratory of Neurodegeneration, Nanjing Medical University, Nanjing 211166,

²Department of Rehabilitation Medicine, First Affiliated Hospital of Nanjing Medical University, Nanjing 210029, China

Subarachnoid hemorrhage (SAH) is a devastating cerebrovascular event that often is followed by permanent brain impairments. It is necessary to explore the pathogenesis of secondary pathological damages in order to find effective interventions for improving the prognosis of SAH. Blockage of brain lymphatic drainage has been shown to worsen cerebral ischemia and edema after acute SAH. However, whether or not there is persistent dysfunction of cerebral lymphatic drainage following SAH remains unclear. In this study, autologous blood was injected into the cisterna magna of mice to establish SAH model. One week after surgery, SAH mice showed decreases in fluorescent tracer drainage to the deep cervical lymph nodes (dcLNs) and influx into the brain parenchyma after injection into the cisterna magna. Moreover, SAH impaired polarization of astrocyte aquaporin-4 (AQP4) that is a functional marker of glymphatic clearance and resulted in accumulations of Tau proteins as well as CD3⁺, CD4⁺, and CD8⁺ cells in the brain. In addition, pathological changes, including microvascular spasm, activation of glial cells, neuroinflammation, and neuronal apoptosis were observed in the hippocampus of SAH mice. Present results demonstrate persistent malfunction of glymphatic and meningeal lymphatic drainage and related neuropathological damages after SAH. Targeting improvement of brain lymphatic clearance potentially serves as a new strategy for the treatment of SAH.

Key words: Subarachnoid hemorrhage, Dural lymphatics, Glymphatic system, Aquaporin 4, Fluorescent tracers

INTRODUCTION

SAH is a devastating cerebrovascular event that can result in a

number of complications, such as brain edema, vasospasm, ischemia, hydrocephalus, and neuroinflammation, causing high mortality and lasting brain impairments [1-4]. Therefore, exploring the mechanisms of its secondary pathological cascades is helpful to find effective strategies for improving the prognosis of SAH.

The paravascular pathway, also termed the glymphatic system, performs pseudo-lymphatic roles in the central nervous system (CNS) [5]. It effectively clears brain metabolic macromolecules via AQP4 water channels that are highly expressed at perivascular astrocyte end-foot processes [6-8]. AQP4 facilitates influx of ce-

Received October 2, 2018, Revised January 25, 2019,
Accepted January 28, 2019

*To whom correspondence should be addressed.
Ming Xiao, TEL: 86-025-8686-2918, FAX: 86-025-8686-2912
e-mail: mingx@njmu.edu.cn
Hongxing Wang, TEL: 86-025-8331-8756, FAX: 86-025-8331-8756
e-mail: wanghongxing@njmu.edu.cn

rebrospinal fluid (CSF) into the brain along para-arterial spaces as well as efflux of interstitial macromolecules out of the brain parenchyma along para-venous spaces [5]. Moreover, human and rodent meninges harbor typical lymphatic vessels that drain macromolecular substances to the dcLNs [9-11]. Therefore, the glymphatic system and meningeal lymphatic vessels may, together, form a functional unit in removal of metabolic waste products from the CNS [12].

Indeed, glymphatic dysfunction causes abnormal accumulation of macromolecules in the brain, which contributes to the occurrence of neurodegenerative disorders, including Alzheimer's disease (AD) [13-16]. Previous studies have also indicated that the paravascular pathway malfunctions following acute stroke [17, 18]. Surgical blockade of meningeal lymphatic drainage via ligation of the dcLNs worsens brain edema and oxidative stress during the acute stage of SAH [19, 20]. However, whether dysfunction of glymphatic and meningeal lymphatic systems persists after SAH remains elusive.

We assumed that, after SAH, blood cells and other components in the subarachnoid space might be drained to the dcLNs through dural lymphatics, subsequently reducing secondary brain damage. Nevertheless, blood clots partially or even totally block this lymphatic drainage route, resulting in blood components entering into and accumulating within the brain perivascular spaces. This in turn impairs clearance function of the glymphatic system, causing accumulation of toxic metabolites and immune components within the brain parenchyma and potentially long-term brain damage. To verify this hypothesis, a mouse SAH model was established by injection of fresh autologous venous blood into the cisterna magna. Our results reveal dysfunction of the glymphatic system and meningeal vessels during the recovery stage after SAH. This finding helps to understand the mechanisms of chronic pathological changes after SAH.

MATERIALS AND METHODS

Animal

Three-month-old male C57/BL6 mice were used in this experiment. All animals were kept in a room of controlled illumination (12:12 h light/dark cycle), humidity (30~50%), and temperature (18~22°C). This study was carried out in accordance with the recommendations of the Institutional Animal Care and Use Committee (IACUC) of Nanjing Medical University.

SAH

SAH model induced by injection of fresh autologous blood into the cisterna magna was adapted from previous reports [21,

22]. Briefly, anesthetized mice were placed in a stereotactic frame. A 1-cm-long incision was made in the posterior neck along the midline, following which paraspinous muscles were separated to expose the atlanto-occipital membrane. A total of 60 μ L of venous blood was drawn from the tail vein using a syringe with a 27-gauge needle (Hamilton, Reno, NV, USA) and injected into the cisterna magna in 10 min by the aid of a micro-manipulator. After injection, the micropipette was then very slowly withdrew. Postoperatively, mice were positioned on an autoregulated electric blanket in a head-down position. This protocol greatly reduced animal deaths and effectively prevented blood leakage from the injection site. In sham control mice, surgery was limited to exposure of the atlanto-occipital membrane. After the animals regained consciousness, they were returned to the cage and feed for one week before behavioral testing.

Neurological score measurement

Neurological scores were blindly examined on the seventh day post SAH using the Garcia scoring system. Several indexes, including spontaneous activity, symmetrical movements of limbs, forepaw outstretching, climbing, body proprioception, and response to vibrissae touch were evaluated [23]. Scoring of each subtest was 0 (worst) to 3 (best). The total score was calculated as a sum of all of the subtest scores.

Open-field test

Mouse spontaneous and anxiety-like behaviors were evaluated in the open field [24]. The animals were placed in the middle of the box (length: 60 cm, width: 60 cm, and height: 25 cm), with an outlined central area (30 cm \times 30 cm) and allowed to move freely for five minutes within the box. The percentage of time spent, number of crosses into the central area, and total distance traveled during the test were measured.

Intracisternal perfusion of fluorescence tracer

Intracisternal injections of Texas Red-dextran (3 kDa) (TR-d3; Thermo Fisher Scientific, Cat #D3328) were described previously [8, 16]. Five μ L of 0.5% TR-d3 resolved in artificial CSF was injected into the cisterna magna. The intracisternal injection was carried out at a rate of 1 μ L/min over five minutes. Thirty minutes after the start of infusion, the anesthetized animals were sacrificed for analyses of TR-d3 diffusion into the brain parenchyma, meningeal lymphatic vessels, and dcLNs.

Brain water content measurement

At one and seven days post surgery, a subgroup of SAH mice and sham control mice were anesthetized, and their brains were

removed, weighed, heated in an oven (70°C) for 72 hours, and re-weighed. The percentage of water content was calculated as [(wet weight–dry weight)/wet weight×100%] [25].

Section preparation

Mice were intraperitoneally deeply anesthetized, then transcardially perfused with 0.9% saline by perfusion pump (Cole-Parmer, USA), followed by 4% paraformaldehyde. Forebrains, meninges, and dcNLs were dissected out and post-fixed overnight at 4°C. The meninges were directly unfolded on a glass slide covered with poly-L-lysine for immunofluorescence. For H&E and immunohistochemical staining, a subset of forebrains was prepared as paraffin sections. Coronal sections at 5 µm were serially cut using a paraffin slicing machine (Leica RM2135, Nussloch, Germany). For analysis of immunofluorescence and TR-d3 diffusion, forebrains and dcNLs were gradient-dehydrated by 20% and 30% sucrose for 24 hours. Tissues were embedded with OTC gel. Then serial sections at 40 µm were cut on a cryostat (Leica CM1900, Nussloch, Germany).

H&E staining

Sections were deparaffinized, rehydrated, and stained with hematoxylin for 5 minutes. The slides were then washed with running water for 10 minutes, followed by counterstaining with eosin for 5 minutes. After differentiation, the sections were dehydrated in 70%, 95%, and 100% ethyl alcohol, followed by being cleared in xylene and permanently mounted.

Immunohistochemistry

Immunohistochemical staining was performed as previously described [26]. In brief, after deparaffinization and hydration, tissue sections were incubated with one of the following primary antibodies: mouse anti-gial fibrillary acidic protein (GFAP; 1:800; Millipore, #AB3594), rabbit anti-ionized calcium-binding adaptor molecule 1 (Iba-1; 1:1000; Wako, #019-19741) and rabbit anti-cysteine-aspartic acid protease 3 (caspase-3; 1:1000; Cell Signaling Technology, #9662) at 4°C overnight. Following PBS wash, sections were incubated with biotinylated-conjugated goat anti-mouse or rabbit IgG (1:200, Vector Laboratories, #BA-1000-1.5; #BA-9200) for one hour at 37°C and then visualized with 3-3'-diaminobenzidine-4 HCl/H₂O₂ (DAB, Sigma-Aldrich, #D0426). Caspase-3 stained sections were counterstained with eosin.

Immunofluorescence

Cryostat sections were blocked for one hour at room temperature with 5% bovine serum albumin, incubated with rabbit anti-fibrin antibody (1:100, Abcam, #ab96532) or a mixture of rabbit

anti-fibrin antibody (1:100, Abcam, #ab96532) and goat anti-AQP4 antibody (1:1000, Millipore, #AB3594) overnight at 4°C. After extensive rinsing, sections were incubated with Alexa Fluor 488 and Alexa Fluor 594 secondary antibodies (Thermo Fisher Scientific, 1:1000, Cat #A-11034; Cat #A-11032) for two hours at room temperature. Meninges were incubated with a monoclonal mouse anti-lymphatic vessel endothelial hyaluronan receptor 1 (LYVE1) antibody (1:1000, Abcam, Cat #ab33682) and thereafter incubated with Alexa Fluor 488 secondary antibody. The slides were washed for 3×5 minutes in PBS containing 1.5 µM 4',6-diamidino-2-phenylindole (DAPI, Invitrogen, #D21490) and then coverslipped with buffered PBS/glycerol.

Cell counting and imaging analysis

All micro-images were captured by a digital microscope (Leica Microsystems, Wetzlar, Germany) and quantified by NIH ImageJ software (Bethesda, MD, USA). For quantification of immunohistochemistry of GFAP, Iba-1, caspase-3 and AQP4, typical hippocampal images were captured in sequence at ×20 objective magnification. The percentage of area covered by GFAP or Iba-1 was measured using interest grayscale threshold analysis with constant settings for minimum and maximum intensities. The percentage area of positive signal was calculated by dividing the area of positive signal to the total hippocampal area. In addition, caspase-3-positive apoptotic cells and total hematoxylin-positive cells in the granular layer of the dentate gyrus were also calculated, and the results were presented as a percentage of apoptosis. The mean AQP4-IR intensity at the regions immediately abutting each vessel and adjacent parenchymal domains, respectively, was measured. AQP4 polarization was obtained by comparing expression ratios of AQP4 at perivascular domains versus parenchymal domains [8, 26]. A mean value of each index mentioned above was calculated for five sections per mouse.

For analysis of TR-d3 penetration into the brain parenchyma, serial images of the whole coronal sections for each animal were obtained at a 1.25×objective magnification. The first section was selected at the beginning at the anterior aspect of the hippocampus, each section was collected every 200 µm apart until a total of five sections had been collected. The percentage area of TR-d3 from the five brain slices was averaged to represent glymphatic CSF influx for each mouse. The percentage area of TR-d3 or fibrin in 2–3 central slides of the dcNLs or in the LYVE1-positive meningeal lymphatic vessels adjacent to the superior sagittal sinus was also analyzed on corresponding images that were obtained under ×20 objective.

In addition, hippocampal microvessels larger than 20 µm in diameter in H&E-stained sections were used for analysis of va-

sospasm. The cross-sectional area of 16~20 microvessels in the bilateral hippocampus per mouse and corresponding perivascular spaces were measured. The results were presented as the ratio of perivascular void area to microvascular area.

Western blotting

Mouse dorsal forebrains (hippocampus and adjacent parietal cortex) were dissected and homogenized in buffer H (1 mM Na HEPES pH7.4, 320 mM sucrose with protease inhibitors). Samples were then resolved on SDS-PAGE and transferred onto PVDF membranes, followed by blocking with 5% nonfat milk dissolved in TBST (pH 7.5, 10 mM Tris-HCl, 150 mM NaCl, and 0.1% Tween 20) at room temperature for 1 hour. Bands were incubated with rabbit polyclonal antibody against interleukin-1 β (IL-1 β ; 1:1000; Millipore; #AB1832P), interleukin 6 (IL-6; 1:1000; Cell Signaling Technology; #12912), tumor necrosis factor- α (TNF- α ; 1:1000; Abcam; #ab6671), caspase-3 (1:1000; Cell Signaling Technology; #9662), Bax (1:1000; Cell Signaling Technology; #2772S), Bcl-2 (1:1000; Cell Signaling Technology; #2876S) or GAPDH (1:1000; Bioworld; #AP0063) at 4°C overnight. Following TBST washing, bands were incubated with horseradish peroxidase-conjugated secondary antibodies (1:3000, ZSGB-BIO; #ZB-2301)

for 1 hour at room temperature, then visualized with ECL Plus detection system. Protein loading and transfer efficiency were balanced with GAPDH. Four or five mice per group in triplicate experiments were averaged to provide a mean value for each group.

Flow cytometry

Mice were perfused from the left cardiac ventricle with cold PBS for 10 minutes. Dorsal forebrains, meninges, and dCLNs were immediately dissected out. Briefly, the skull was separated into the upper half and lower half utilizing microsurgical scissors. The upper part of meninges was carefully separated from the medial surface of the cranium. For collecting the dCLNs, a longitudinal incision was made on the neck from the mandible to the sternum, and the dCLNs were able to be found under the lower part of the sternoclavicular muscles [16]. The meningeal tissues were dissected with fine forceps and digested in RPMI-1640 medium (Sigma-Aldrich, Cat #R0883) containing 1.4 U/ml Collagenase VIII (Sigma-Aldrich, Cat #C2139) and 1 mg/ml DNase1 (Sigma-Aldrich, Cat #11119915001) for 15 minutes at 37°C. The dorsal forebrains and dCLNs were smashed in Dulbecco's Modified Eagle Medium (DMEM) containing 10% fetal calf serum. Digested meninges and smashed forebrains and dCLNs were dissociated using

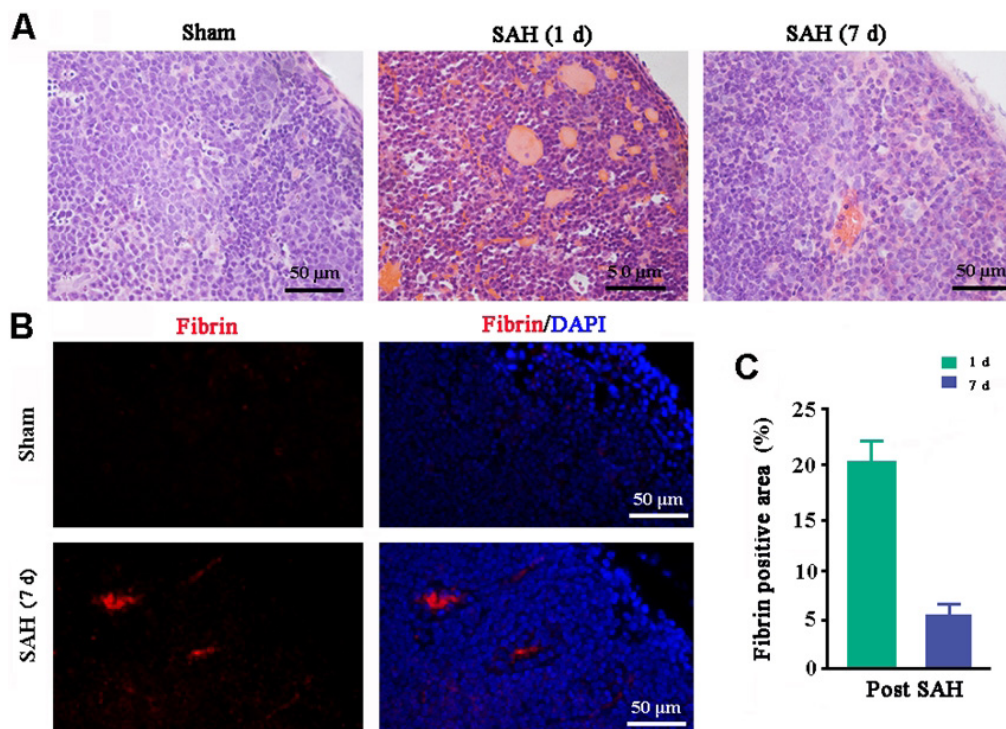


Fig. 1. Drainage of blood cells and components to the dCLNs following injection into the cisterna magna. (A) H&E staining showed that a hemoglobin-like substance was absent in the intact dCLNs but clearly observed in the dCLNs at 1 day post SAH and significantly decreased at 7 days post SAH. (B) Fibrin-positive signals were still present within the dCLNs of SAH mice at 7 days post SAH. (C) Percentage of fibrin-positive area within the dCLNs at 1 and 7 days after SAH. Results expressed as mean \pm SEM from 4 mice per group.

pipetting, then passed through 70- μ m filters. Cell suspension was incubated with antibody dye CD3 (1:400, eBioscience, Cat #145-2C11), CD4 (1:400, eBioscience Cat #17-0041-83), or CD8 (1:400, BD Bioscience Cat #335787) for 30 minutes at 4°C. Data were acquired on an LSR II cytometer (BD Biosciences, Franklin Lakes, NJ, USA) and analyzed using FlowJo Pro software (FlowJo, LLC, Ashland, OR, USA). The number of cells used for each analysis was 10,000 for meningeal samples and 50,000 for forebrains and dCLNs. Mean value of each sample was obtained from three independent experiments.

Statistical analysis

Statistical analyses were conducted using SPSS software, version 19.0 (SPSS Inc., USA). The data were analyzed by Student's t-test and expressed as mean \pm SEM. Pearson correlation analysis was calculated to evaluate the link between the number of apoptotic cells and cerebral vasospasms in the hippocampus. Correlation between overall behavior score and percentage area of TR-d3 within

the brain was also analyzed by Pearson correlation analysis.

RESULTS

Intracisternally injected blood cells are drained to the dCLNs

A large number of blood cells had accumulated within the dCLNs one day after injection of autologous blood into the cisterna magna of mice. At one week post SAH, a small amount of a hemoglobin-like substance was still observed within the dCLNs (Fig. 1A). Fibrin is a fibrous, non-globular protein involved in the clotting of blood. Quantification of fibrin immunofluorescence in the dCLNs demonstrated the percentage of fibrin-positive area was 20.8% at one day and 5.24% at one week post SAH, respectively (Fig. 1B and 1C). Neither blood cells nor fibrin was found in the dCLNs of sham control mice (Fig. 1A~C). These results suggest that blood cells are able to be drained to the dCLNs after injection into the cisterna magna.

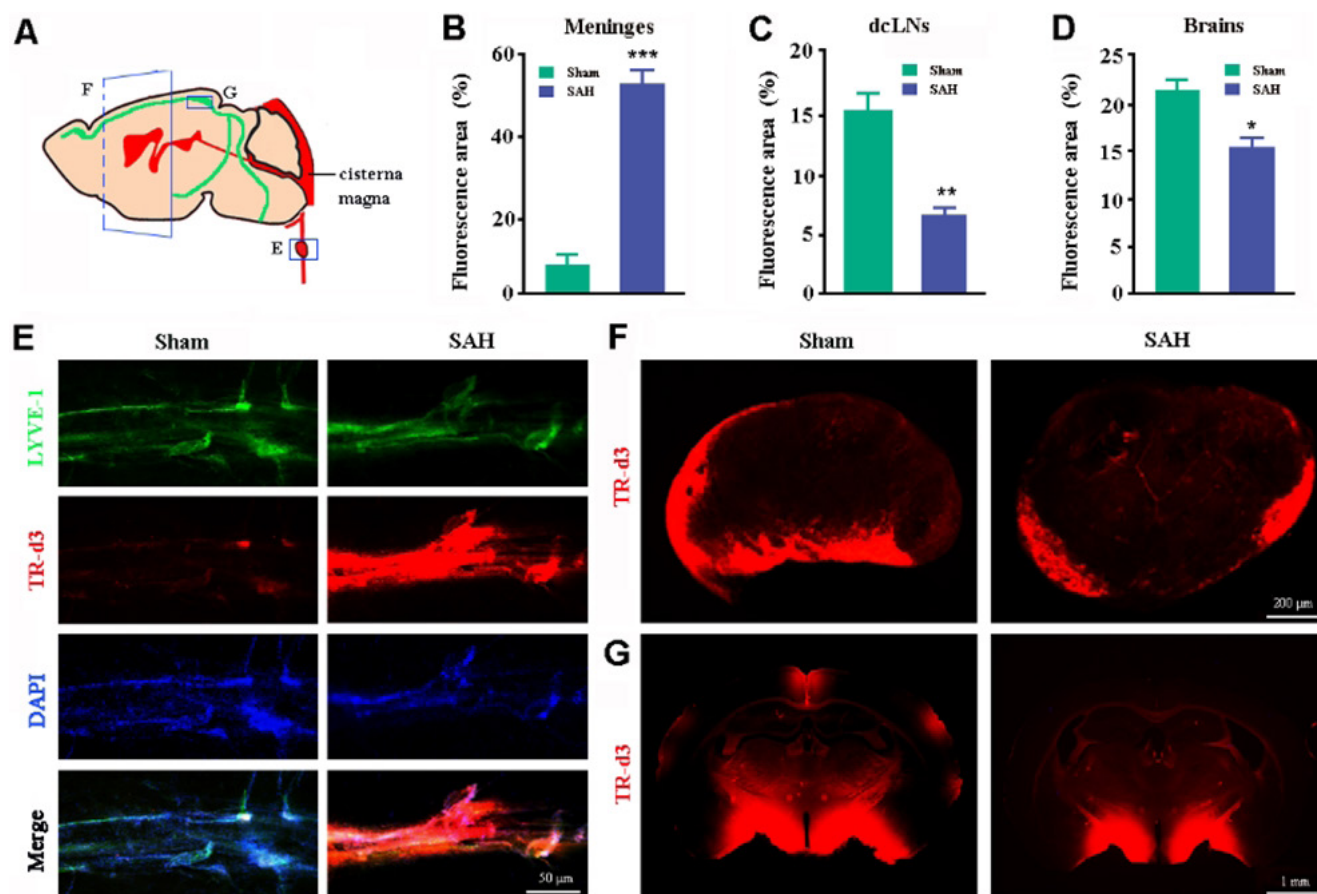


Fig. 2. Analyses of glymphatic and meningeal lymphatic drainage. (A) Schematic diagram of measuring distribution of TR-d3 within the dCLNs, brain parenchyma, and meningeal lymphatic vessels at 30 min after injection into the cisterna magna. (B~G) Quantitation and representative images of TR-d3 fluorescence within LYVE-1 positive meningeal lymphatic vessels (B and E), dCLNs (C and F), and forebrain (D and G). Data shown as mean \pm SEM from 4 mice per group. Statistical analysis was performed by Student's t-test. * p <0.05, ** p <0.01, *** p <0.001.

Lymphatic clearance malfunction and Tau protein aggregation in SAH mice

Previous studies, including one from our group, have confirmed that meningeal lymphatic vessels absorb brain macromolecules and tracers from the subarachnoid space for transport into the dCLNs [10, 15, 16]. In order to determine whether long-term lymphatic clearance dysfunction occurs during SAH, a fluorescent tracer TR-d3 was injected into the cisterna magna one week after surgery (Fig. 2A). In sham control mice, a very small amount of TR was attached to the walls of LYVE1-positive lymphatic vessels adjacent to the superior sagittal sinus (Fig. 2E), while a large amount of tracer penetrated into the dCLNs (Fig. 2F), suggesting that meningeal lymphatic vessels can quickly absorb CSF macromolecular substances and drain them downstream into dCLNs. The superior sagittal lymphatic vessels were almost full with TR-d3 in SAH mice (Fig. 2E), while penetration of TR-d3 in the dCLNs was significantly less than that of sham controls (Fig. 2F). Quantitative analysis revealed that the percentage of TR-d3-positive area in the lymphatic vessels of the superior portions of the skulls of SAH mice was almost eight times that of sham controls ($p=0.0012$; Fig. 2B). By contrast, the percentage of TR-d3 positive area in dCLNs of SAH mice was only 43.48% of that of sham controls ($p=0.0124$;

Fig. 2C). These data suggest that SAH persistently impairs draining ability of meningeal lymphatic vessels. Moreover, recent studies have revealed a functional connection between the glymphatic system and meningeal lymphatic vessels. Brain influx of CSF macromolecules through the paravascular pathway is impaired when meningeal lymphatic drainage is disrupted [15, 16]. In agreement with this, SAH mice showed a significant decrease in penetration of intracisternally injected TR-d3 into the brain parenchyma ($p=0.0124$ versus sham controls; Fig. 2D and 2G).

Consistent with dysfunction of glymphatic clearance, there was an abnormal enlargement of the perivascular space in the brain of SAH mice, as revealed by significant increases in the ratio between perivascular void area and vascular area ($p=0.0018$, versus sham controls; Fig. 3A~B). Glymphatic dysfunction in SAH mice was further confirmed by high levels of brain total Tau and phosphorylated Tau, PHF-1 ($p=0.0058$; $p=0.0227$, versus sham controls, respectively; Fig. 3D~E). Brain edema is a common complication of acute SAH [3]. An earlier study reported that brain water content is increased significantly in 1~3 days post SAH and brain edema is further aggravated following LdcLNs [19]. However, whether long-term dysfunction of cerebral lymphatic drainage is involved in brain edema after SAH has not been addressed. In the present

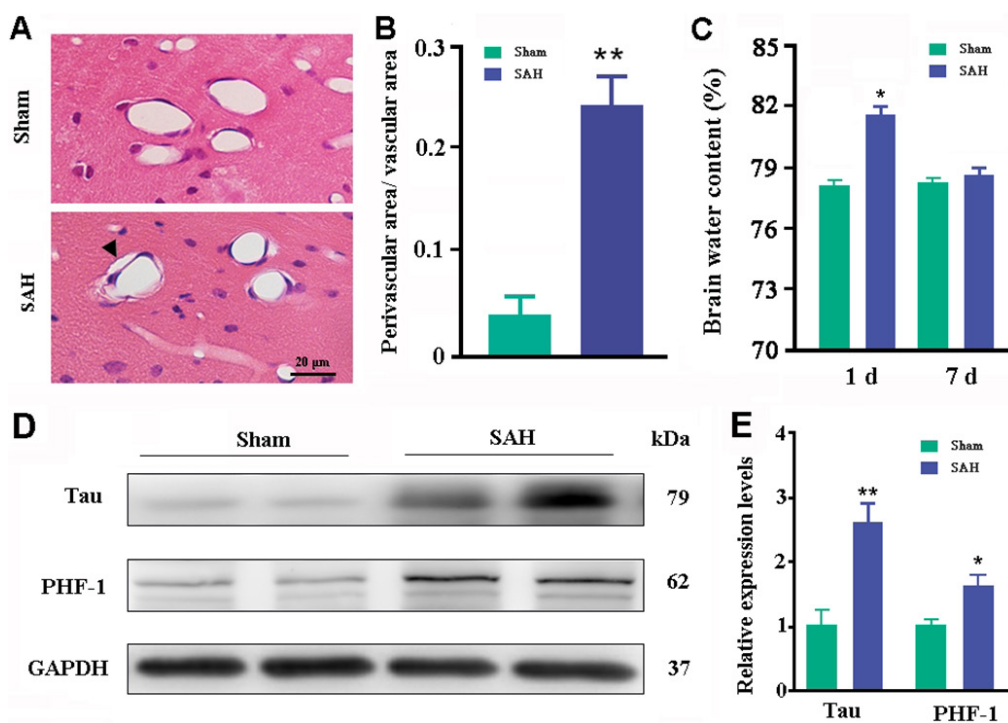


Fig. 3. Analyses of paravascular area, brain water content, and Tau levels. (A) H&E staining showed that hippocampal blood vessels had smaller inner diameters with increased perivascular space (arrowhead) at 7 days post SAH. (B) Ratio of perivascular area/vascular area. (C) Percentage of brain water content at 1 and 7 days after SAH. (D~E) Representative bands of Western blotting and corresponding densitometry analysis for expression levels of total Tau protein and phosphorylated Tau protein (PHF-1) in the dorsal forebrain at 7 days post SAH. Graphs are the summary of results from three independent experiments. Data shown as mean±SEM from 4 mice per group. The statistical analysis was performed by Student's t-test. * $p<0.05$, ** $p<0.01$.

study, we demonstrated that brain water content was significantly higher one day post SAH ($p=0.023$, versus sham controls) but returned to normal levels at seven days ($p=0.1813$; Fig. 3C). This suggests an effective compensatory mechanism for maintaining CNS water homeostasis during the recovery period of SAH. Taken

together, the above results support the view that brain macromolecule clearance is more dependent on the dural lymphatic system than CSF clearance [10, 15].

Dural lymphatic vessels are also responsible for draining lymphocytes from CSF into the peripheral lymph nodes [11, 16, 27].

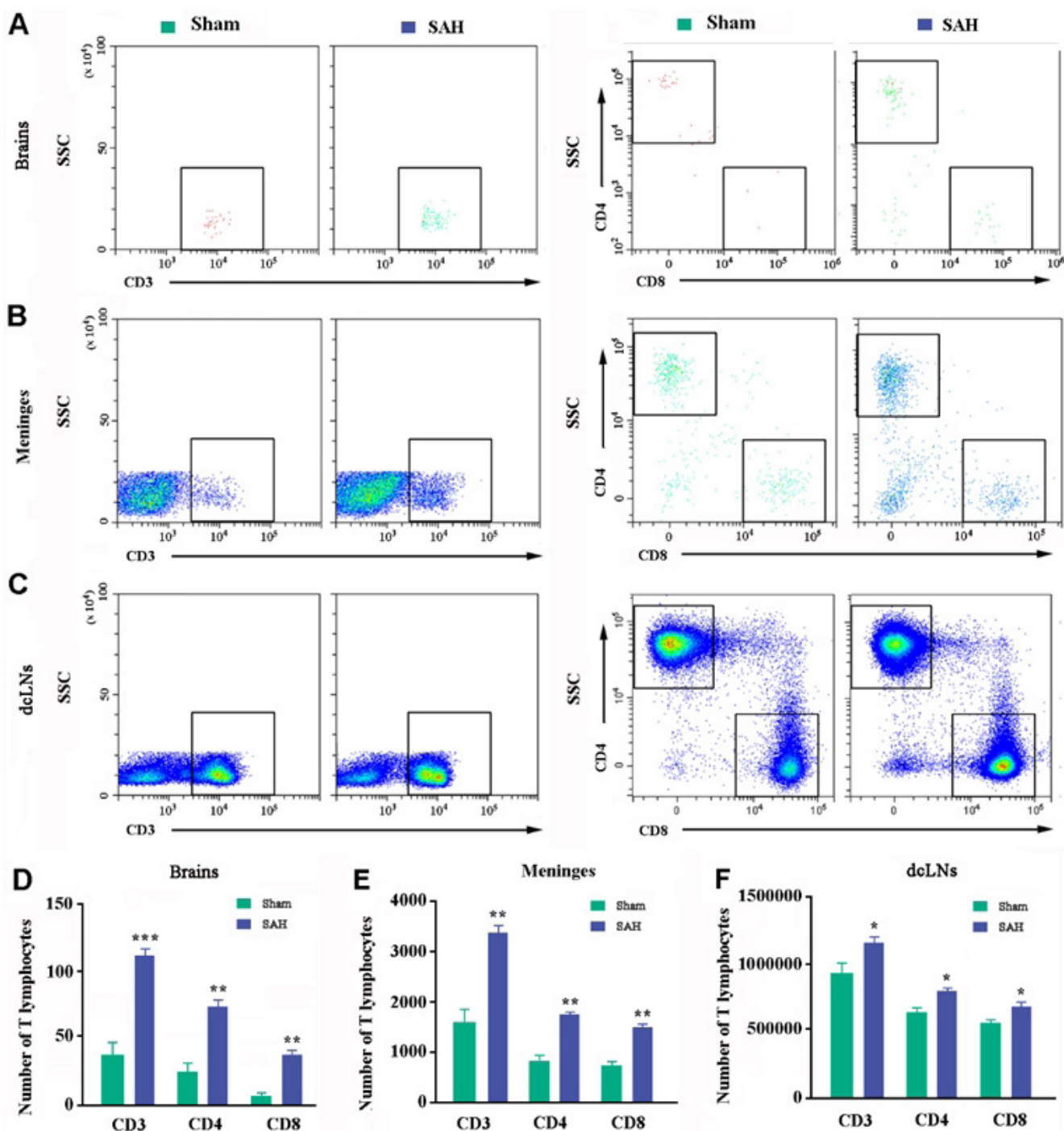


Fig. 4. Analysis of T cells in the brains, meninges, and dLNs. (A~F) Representative dot plot and quantification of CD3⁺, CD8⁺, and CD4⁺ T cells in the dorsal forebrain (A and D), meningeal (B and E), and dLNs samples (C and F). Graphs are the summary of results from two independent experiments. Data shown as mean±SEM from 4 mice per group. Statistical analysis was performed by Student's t-test, $n=4$. * $p<0.05$, ** $p<0.01$, *** $p<0.001$.

Flow cytometry analysis showed that the number of CD3⁺, CD4⁺, and CD8⁺ cells within the brain parenchyma ($p=0.0264$, $p=0.0138$, $p=0.0265$, respectively; Fig. 4A and 4D) and meninges ($p=0.0264$, $p=0.0138$, $p=0.0265$, respectively; Fig. 4B and 4E) of SAH mice was more than twice that of the sham controls, respectively. CD3⁺, CD4⁺, and CD8⁺ cell counts were also mildly increased in SAH-dcLNs ($p=0.0482$, $p=0.0184$, $p=0.0191$, versus sham controls, respectively; Fig. 4C and 4F). Together, the above evidence demonstrates that there is a long-lasting malfunction of meningeal lymphatic clearance with abnormal accumulation of macromolecules and lymphocytes within the brain parenchyma during SAH.

Impaired AQP4 polarity after SAH

Previous studies have shown that glymphatic clearance function depends on highly selective expression of AQP4 on microvascular

end-feet of astrocytes [6-8]. Therefore, we queried whether impaired glymphatic malfunction is associated with altered AQP4 polarization. Abnormal AQP4 polarization was observed in the hippocampus one week post SAH (Fig. 5A). Quantitative analysis showed that SAH increased immunoreactive intensity of AQP4 ($p=0.004$, versus sham controls; Fig. 5B) but decreased perivascular polarity of AQP4 ($p=0.019$, versus sham controls; Fig. 5C). Consistently, Western blot showed that SAH increased AQP4 expression levels in the dorsal forebrain ($p=0.021$, versus sham controls; Fig. 5D~E).

Mild reactivation of glial cells and neuroinflammation after SAH

Both astrocytes and microglia participate in maintaining brain homeostasis and respond to various types of injuries [27, 28].

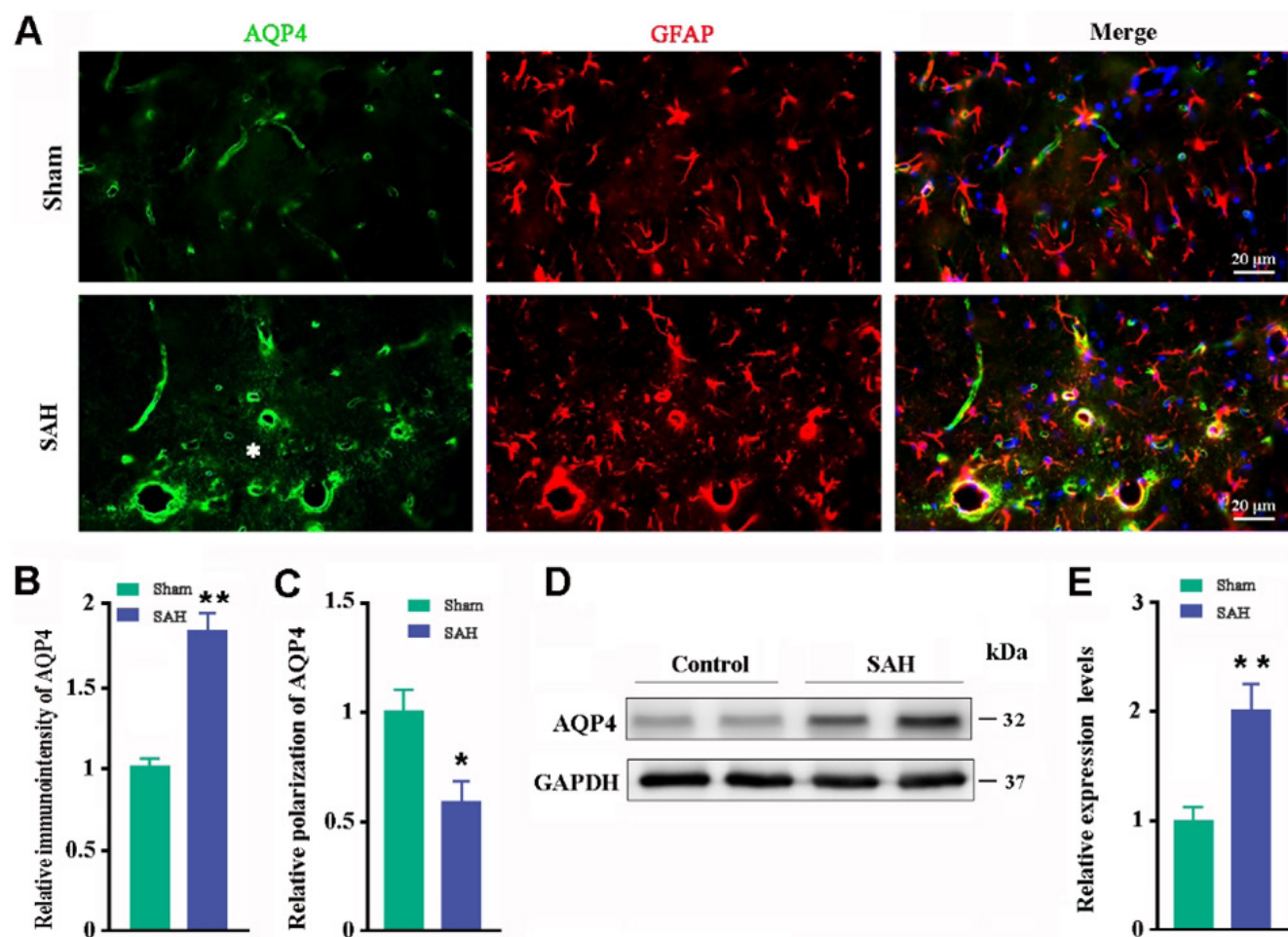


Fig. 5. Analyses of AQP4 polarization and expression. (A) Immunofluorescent staining of AQP4 in the hippocampus. An abnormal increase in AQP4 expression was observed in the parenchymal domains (star) of SAH mice. (B) Relative pixel intensity of AQP4 immunofluorescence. (C) Relative perivascular polarization of AQP4. (D~E) Representative bands of Western blotting and corresponding densitometry analysis for expression levels of AQP4 in the dorsal forebrain from three independent experiments. Results expressed as mean \pm SEM from 4 mice per group. The statistical analysis was performed by Student's t-test. * $p<0.05$; ** $p<0.01$.

Immunohistochemical staining revealed that Iba-1-positive microglia and GFAP-positive astrocytes in sham control mice were under resting state. In SAH mice, astrocytes and microglia were mildly activated with intense staining and increased cell size (Fig. 6A). Quantitative data revealed that SAH mice had high percentages of Iba-1-positive and GFAP-positive area in the hippocampus ($p=0.0082$; $p=0.0227$, versus sham controls respectively; Fig. 6B~C). Consistent with activation of glial cells, levels of IL-1 β , IL-6, and TNF- α were high in the dorsal forebrain of SAH mice, compared with those in sham controls ($p=0.006$, $p=0.001$, $p=0.007$, respectively; Fig. 6D~E).

Neuronal apoptosis and neurological deficits of SAH mice

Consistent with microvascular spasm and glial inflammation, neuronal apoptosis occurred in the hippocampus of SAH mice (Fig. 7A). The percentage of cysteine-aspartic acid protease 3 (caspase-3) positive neurons in the hippocampal dentate gyrus of SAH mice was 3.7 times greater than that of sham controls (Fig. 7B). Western blot also revealed that expression levels of apoptosis-related proteins, cleaved caspase-3, and Bax increased, while anti-apoptosis protein Bcl-2 decreased in the dorsal forebrain of SAH mice ($p=0.0167$, $p=0.0053$, $p=0.0286$, versus sham controls, respec-

tively; Fig. 7C~D).

Neurological deficits and psychiatric symptoms are common during the recovery of patients with SAH as well as SAH animal models [1-4]. Neurological scores of SAH mice were lower than those of sham controls ($p=0.0346$; Fig. 8A). We also evaluated mouse spontaneous exploratory and anxiety-like behaviors by use of the open field test. These tests showed that SAH mice had significantly reduced time spent in and number of entrances into the central area and total distance traveled, as compared with sham controls ($p=0.0465$, $p<0.0001$, $p=0.0332$, respectively; Fig. 8B~D).

Correlation between glymphatic dysfunction and neurological deficits

Interestingly, correlation analysis indicates that the number of apoptotic cells is closely related to cerebral vasospasm in the hippocampus ($r=0.908$; $p=0.0018$; Fig. 9A). In addition, there was a positive correlation between overall behavior score and percentage area of TR-d3 within the brain ($r=0.8913$, $p=0.003$; Fig. 9B). These results suggest that dysfunction of the glymphatic system is involved in neuronal apoptosis and neurological deficits after SAH.

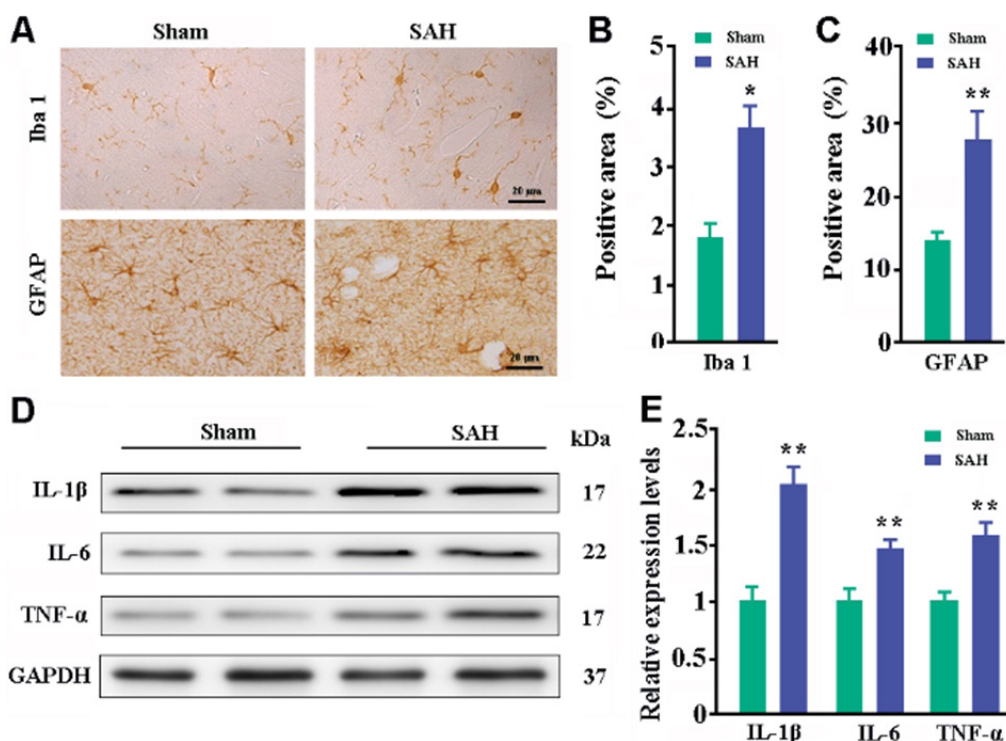


Fig. 6. Analyses of glial activation and neuroinflammation. (A) Immunohistochemical staining for Iba-1 and GFAP in the hippocampus. (B) Percentage of Iba-1-positive area. (C) Percentage of GFAP-positive area. (D~E) Representative bands of Western blot and corresponding densitometry analysis for expression levels of IL-1 β , IL-6, and TNF- α in the dorsal forebrain from three independent experiments. Data expressed as mean \pm SEM from 4 (B and C) or 5 (D) mice per group. Statistical analysis was performed by Student's t-test. * $p<0.05$, ** $p<0.01$.

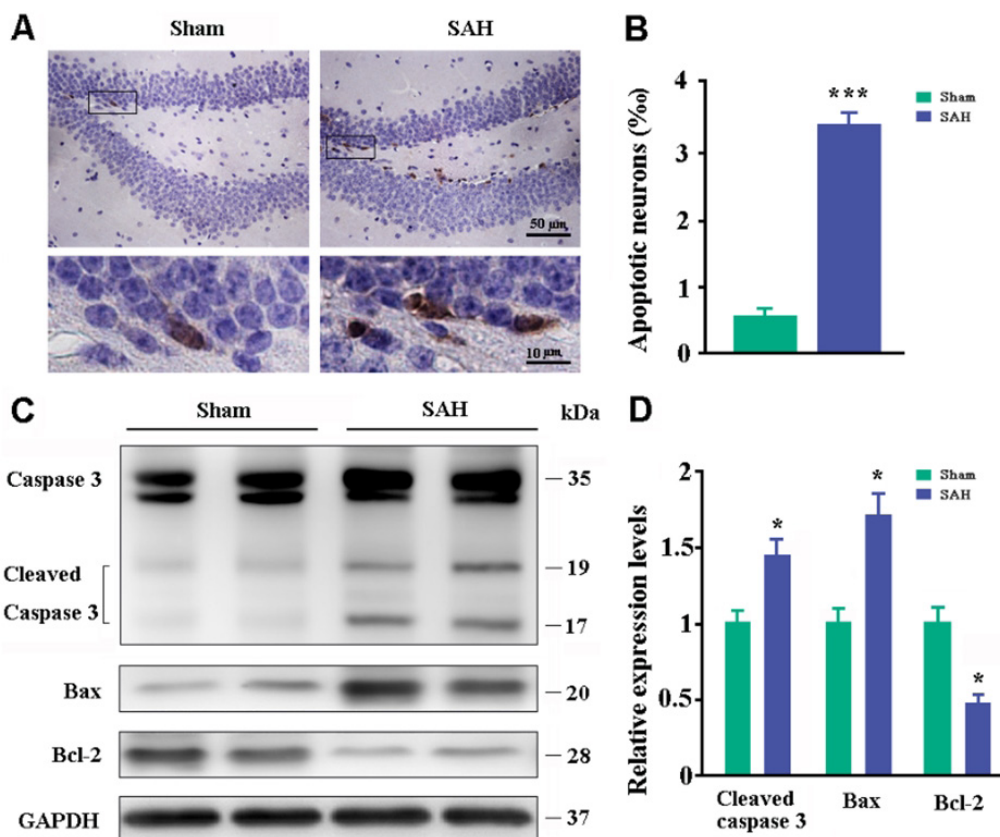


Fig. 7. Analyses of neuronal apoptosis. (A) Immunohistochemical staining for caspase-3 in the dentate gyrus of hippocampus. (B) Percentages of caspase-3-positive apoptotic neurons. (C-D) Representative bands of Western blot and corresponding densitometry analysis for expression levels of cleaved caspase-3, Bax, and Bcl-2 in the dorsal forebrain. Graphs are the summary of results from three independent experiments. Data expressed as mean±SEM from 4 (B) or 5 (D) mice per group. Statistical analysis was performed by Student’s t-test. *p<0.05, ***p<0.001.

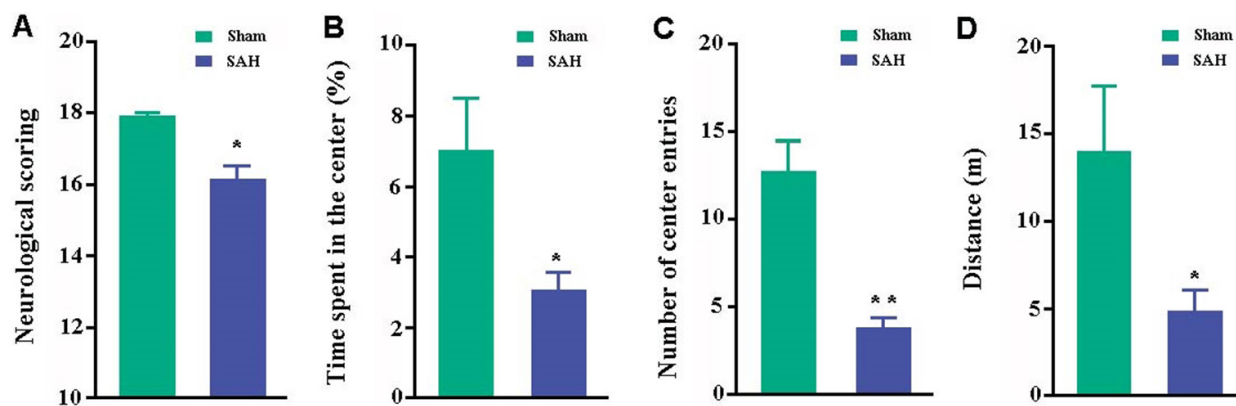


Fig. 8. Behavioral analyses. (A) Garcia neurological scores. (B) Percentage of time spent in the central area of the open field. (C) Number of entries into the central area. (D) Total distance traveled during the test. Data represent mean±SEM from 8 mice per group. Data in figures were analyzed by Student’s t-test. *p<0.05, **p<0.01.

DISCUSSION

Multiple complications may be involved in the pathological course of SAH [2]. Recent studies have reported that the glym-

phatic system is damaged during the acute phase of SAH and ischemic stroke [19, 20]. In the present study, a mild model of SAH is established by a one-time injection of autologous venous blood into the cisterna magna of mice, successfully avoiding ani-

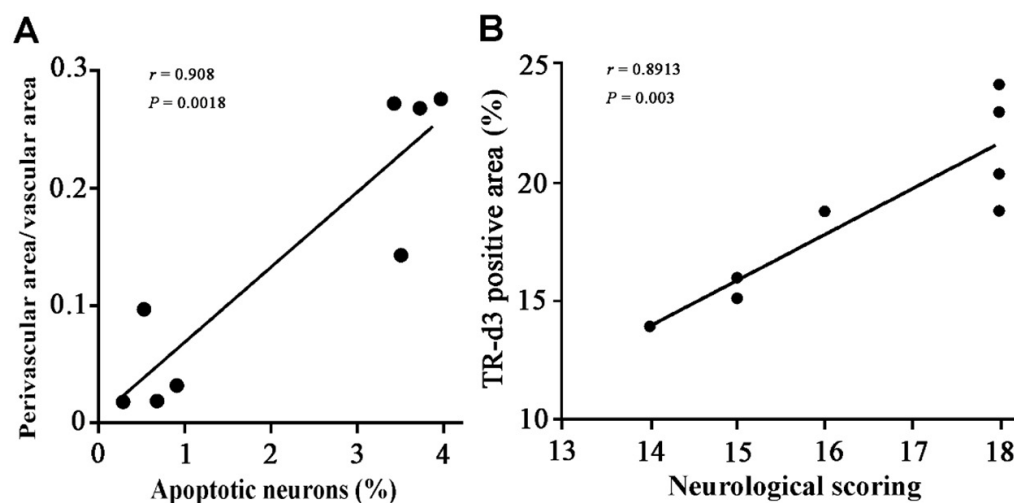


Fig. 9. Correlation analysis data. (A) The extent of cerebral vasospasm positively correlated with the number of apoptotic cells in the hippocampus. (B) Percentage of CSF tracer influx into the brain parenchyma partially correlated with overall behavior score. Data from 4 SAH mice and 4 sham controls, analyzed by Pearson correlation analysis.

mal death [22]. By use of this SAH model, we have demonstrated dysfunction of the glymphatic and meningeal lymphatic drainage mechanism during the recovery period of SAH.

Recently, a typical lymphatic structure has been identified in both human and mouse meninges, mediating drainage of macromolecular substances and lymphocytes from the CNS to the peripheral circulation [9-11, 15, 16]. In the present study we have provided evidence that meningeal lymphatic vessels can drain intracisternally injected blood cells into the dLNs, which may ameliorate secondary impairments following SAH. Earlier studies have reported that blocking cerebral lymphatic drainage worsens brain oxidative stress, cerebral blood flow, and brain edema in the acute phase of SAH [19, 20]. We have further demonstrated an obstruction of dural lymphatic drainage at one week post SAH, revealed by significantly decreased transit of intracisternally injected TR-3d toward the dLNs and abnormal accumulation of Tau and T cells within the brain parenchyma and meninges of mice.

We also have demonstrated a long-lasting glymphatic malfunction in the SAH model, which may be associated with abnormal aggregation of blood cells and blood components within the brain perivascular spaces as well as activated astrocytes with loss of AQP4 polarization. It has been known that the glymphatic pathway mediates clearance of macromolecules out of the brain parenchyma and depends on perivascular polarization of AQP4 [6, 7]. Under normal physiological conditions, driven by arterial pulsation, CSF penetrates into the brain parenchyma to form interstitial fluid (ISF), which flows into the subarachnoid space through the para-venous pathway (Fig. 10A). Soluble macromolecular metabolites are removed out of the brain parenchyma along with the bulk flow of ISF [14]. As the most abundant water channel in the CNS, AQP4 mediates rapid influx of CSF into the brain and subsequent efflux of ISF into the subarachnoid space, potentially serving as the

main driving force for ISF bulk flow [14]. In various states, such as aging [6], brain contusion [7], and AD [15, 16], astrocytes are activated, resulting in abnormal expression of AQP4 on astrocyte soma and processes around neuronal elements. Almost all SAH complications, including cerebral vasospasm, microcirculatory disturbance, microthrombosis, cerebral ischemia, hypoxia, and oxidative stress, can lead to astrocyte activation [1, 2, 19, 20, 29-31]. Impairing vascular polarization of AQP4 has been shown to hamper glymphatic clearance of metabolic macromolecules, including A β and Tau, from the brain [6, 7]. We have reported that blockade of meningeal lymphatic drainage or AQP4 deletion exacerbates AD-like pathology in APP/PS1 mice [16, 26]. Our recent study has revealed that brain A β and Tau levels are markedly increased in AQP4^{-/-} mice following ligation of dLNs [32]. These data indicate that inhibiting mislocalization of astrocyte AQP4 might be an effective treatment target to protect glymphatic function in various neurological diseases associated with abnormal aggregation of brain macromolecules [33].

As mentioned above, besides removal of brain macromolecular metabolites, dural lymphatic vessels drain CSF lymphocytes to the dLNs [10, 15, 16]. The present study has shown that CD3-, CD4-, and CD8-positive T cells accumulate in the brain parenchyma and meninges in SAH mice. These excessive T cells might have originated from intracisternally injected blood cells and accumulated as a consequence of impaired cerebral lymphatic drainage. Recent studies have suggested that the meningeal lymphatics-dLNs route is crucial for the homeostasis of brain-immune interactions, and its abnormality is involved in the pathogenesis of immune-related neurological diseases [12, 34]. Notably, the normal flow of meningeal T cells is interrupted in mice after surgical removal of dLNs, resulting in cognitive dysfunction in the water maze test [35]. Based on this, long-lasting impairment of meningeal T cell hom-

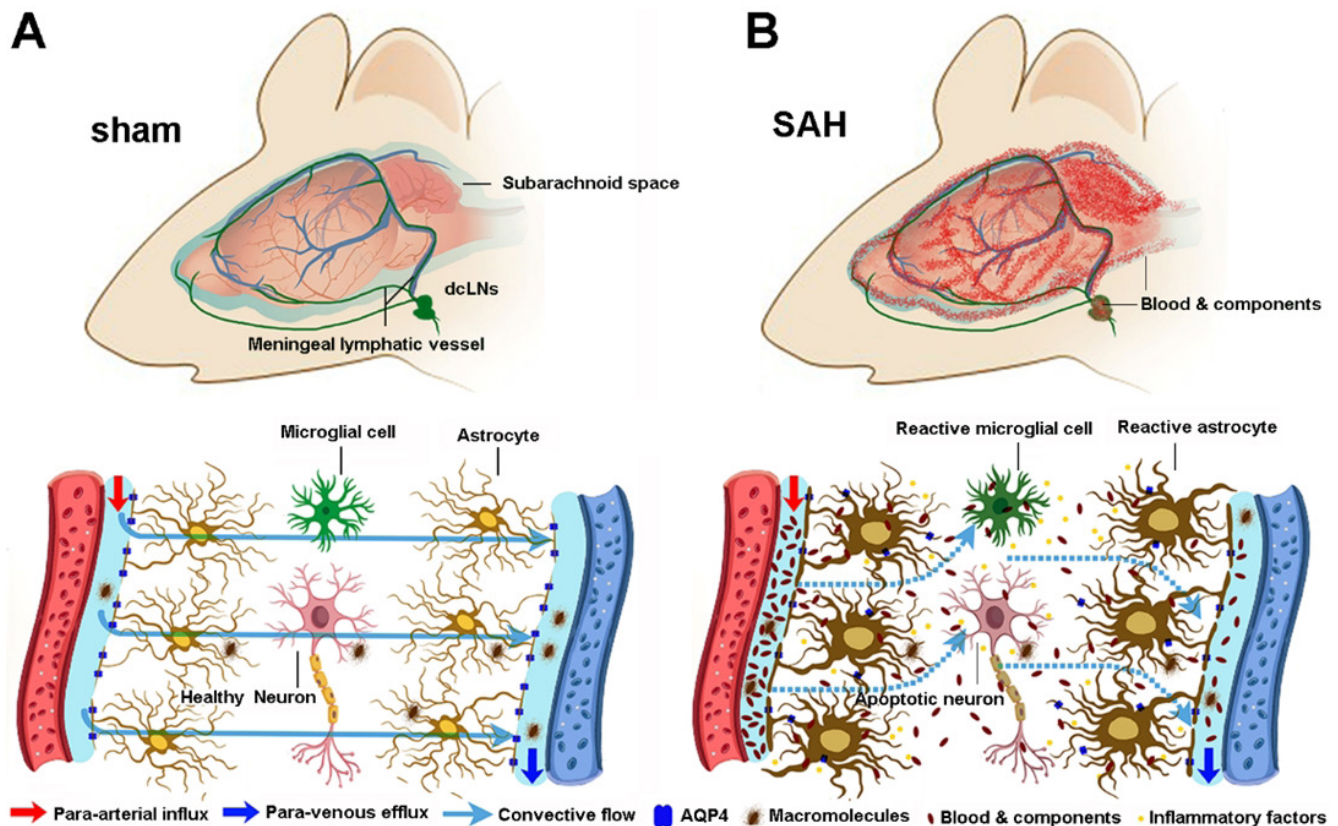


Fig. 10. Schematic diagram of malfunction of glymphatic and meningeal lymphatic drainage post SAH. (A) Under intact conditions, perivascular AQP4 mediates convective flow from para-arterial to para-venous spaces, thus facilitating drainage of brain macromolecular substances to the dCLNs via meningeal lymphatic vessels. (B) After SAH, blood clots block the meningeal lymphatic drainage route, resulting in blood cells and components entering into and accumulating within brain perivascular spaces. This in turn impairs glymphatic clearance function, causing accumulation of toxic metabolites and immune components within the brain parenchyma as well as long-term brain damage.

ing might be involved in persistent neurological deficits after SAH.

Interestingly, compared with abnormal accumulation of macromolecular substances and immune cells within the brain parenchyma, the brain water content returns to normal levels at 7 days after SAH, although polarization of AQP4 and intracisternal CSF tracer influx and clearance remain abnormal. Consistent with the present results, in a closed-skull model of murine traumatic brain injury (TBI), intracranial pressure and cerebral edema peak 1–3 days post injury and largely normalize by 7 days post injury. Increased AQP4 expression and loss of polarized localization of AQP4 at endfoot processes of reactive astrocytes increases up to 1 week post injury, and remains dysregulated by 4 weeks post injury [36]. A subsequent study further confirmed that in addition to facilitating resolution of vasogenic edema after TBI, the long-term mislocalization of AQP4 impairs glymphatic clearance function, contributing to tau aggregation and neurodegeneration in the chronic phase after TBI [7]. These data suggest that adaptive changes in CSF clearance occur after the compromise of glym-

phatic and meningeal lymphatic systems.

This speculation is further supported by the evidence that mice born without meningeal lymphatic vessels show normal brain interstitial fluid pressure and water content [10]. A recent study from our group also revealed that brain water content is not changed significantly in either AQP4 knockout mice or wild-type mice at 3 days and 2 weeks after ligation of dCLNs. By contrast, no matter received ligation of dCLNs or not, AQP4 knockout mice show mildly high brain water content, relative to WT controls [32]. In agreement with our results, whole or astroglial conditional AQP4 knockout mice established by other groups also exhibit a slight increase in global brain water content [37–39]. Although AQP4 absence mildly increases brain water content and interstitial volume, loss of perivascular AQP4 polarization in the aging brain relates to a reduction in CSF-ISF exchange, but does not affect brain extracellular space [6]. Moreover, brain water content subtly declines with age in healthy humans [40, 41] as well as in mice [42]. These results indicate that AQP4 polarity dependent glymphatic trans-

port facilitates the clearance of excess fluid and macromolecules from the brain parenchyma, but is not the sole determinant for the basal brain water content, because water movement into, through and out of the brain is via various routes and mechanisms [43]. In summary, cerebral edema caused by SAH gradually subsides over time, which might be due to multiple compensation pathways, including increased transport of water across the blood-brain barrier, transport of arachnoid granulations into the circulatory system, and decreases in CSF production from the ventricular choroid plexus [43]. To confirm this presumption, further work is needed.

In conclusion, the present study has revealed lymphatic drainage dysfunction and related neuropathological changes in the recovery period of SAH model (Fig. 10B). It would be interesting to determine if improving drainage of the dural lymphatic vessels could effectively mitigate secondary pathological processes and eliminate neuropsychiatric sequelae of SAH. The potential results will help to further reveal the pathophysiological mechanisms of SAH and provide an experimental basis for improving the prognosis of SAH via targeting the lymphatic clearance system.

ACKNOWLEDGEMENTS

This work was supported by grants from the National Natural Science Foundation of China (81671070 and 8177090958).

REFERENCES

- Chen S, Luo J, Reis C, Manaenko A, Zhang J (2017) Hydrocephalus after subarachnoid hemorrhage: pathophysiology, diagnosis, and treatment. *BioMed Res Int* 2017:8584753.
- El Amki M, Dubois M, Lefevre-Scelles A, Magne N, Roussel M, Clavier T, Guichet PO, Gérardin E, Compère V, Castel H (2018) Long-lasting cerebral vasospasm, microthrombosis, apoptosis and paravascular alterations associated with neurological deficits in a mouse model of subarachnoid hemorrhage. *Mol Neurobiol* 55:2763-2779.
- Sehba FA, Hou J, Pluta RM, Zhang JH (2012) The importance of early brain injury after subarachnoid hemorrhage. *Prog Neurobiol* 97:14-37.
- Turan N, Miller BA, Heider RA, Nadeem M, Sayeed I, Stein DG, Pradilla G (2017) Neurobehavioral testing in subarachnoid hemorrhage: a review of methods and current findings in rodents. *J Cereb Blood Flow Metab* 37:3461-3474.
- Plog BA, Nedergaard M (2018) The glymphatic system in central nervous system health and disease: past, present, and future. *Annu Rev Pathol* 13:379-394.
- Kress BT, Iliff JJ, Xia M, Wang M, Wei HS, Zeppenfeld D, Xie L, Kang H, Xu Q, Liew JA, Plog BA, Ding F, Deane R, Nedergaard M (2014) Impairment of paravascular clearance pathways in the aging brain. *Ann Neurol* 76:845-861.
- Iliff JJ, Chen MJ, Plog BA, Zeppenfeld DM, Soltero M, Yang L, Singh I, Deane R, Nedergaard M (2014) Impairment of glymphatic pathway function promotes tau pathology after traumatic brain injury. *J Neurosci* 34:16180-16193.
- Iliff JJ, Wang M, Liao Y, Plogg BA, Peng W, Gundersen GA, Benveniste H, Vates GE, Deane R, Goldman SA, Nagelhus EA, Nedergaard M (2012) A paravascular pathway facilitates CSF flow through the brain parenchyma and the clearance of interstitial solutes, including amyloid β . *Sci Transl Med* 4:147ra111.
- Absinta M, Ha SK, Nair G, Sati P, Luciano NJ, Palisoc M, Louveau A, Zaghoul KA, Pittaluga S, Kipnis J, Reich DS (2017) Human and nonhuman primate meninges harbor lymphatic vessels that can be visualized noninvasively by MRI. *ELife* 6:e29738.
- Aspelund A, Antila S, Proulx ST, Karlsen TV, Karaman S, Detmar M, Wiig H, Alitalo K (2015) A dural lymphatic vascular system that drains brain interstitial fluid and macromolecules. *J Exp Med* 212:991-999.
- Louveau A, Smirnov I, Keyes TJ, Eccles JD, Rouhani SJ, Peske JD, Derecki NC, Castle D, Mandell JW, Lee KS, Harris TH, Kipnis J (2015) Structural and functional features of central nervous system lymphatic vessels. *Nature* 523:337-341.
- Louveau A, Plog BA, Antila S, Alitalo K, Nedergaard M, Kipnis J (2017) Understanding the functions and relationships of the glymphatic system and meningeal lymphatics. *J Clin Invest* 127:3210-3219.
- Peng W, Achariyar TM, Li B, Liao Y, Mestre H, Hitomi E, Regan S, Kasper T, Peng S, Ding F, Benveniste H, Nedergaard M, Deane R (2016) Suppression of glymphatic fluid transport in a mouse model of Alzheimer's disease. *Neurobiol Dis* 93:215-225.
- Tarasoff-Conway JM, Carare RO, Osorio RS, Glodzik L, Butler T, Fieremans E, Axel L, Rusinek H, Nicholson C, Zlokovic BV, Frangione B, Blennow K, Ménard J, Zetterberg H, Wisniewski T, de Leon MJ (2015) Clearance systems in the brain: implications for Alzheimer disease. *Nat Rev Neurol* 11:457-470.
- Da Mesquita S, Louveau A, Vaccari A, Smirnov I, Cornelison RC, Kingsmore KM, Contarino C, Onengut-Gumuscu S, Farber E, Raper D, Viar KE, Powell RD, Baker W, Dabhi N, Bai R, Cao R, Hu S, Rich SS, Munson JM, Lopes MB, Overall CC, Acton ST, Kipnis J (2018) Functional aspects of men-

- ingeal lymphatics in ageing and Alzheimer's disease. *Nature* 560:185-191.
16. Wang L, Zhang Y, Zhao Y, Marshall C, Wu T, Xiao M (2018) Deep cervical lymph node ligation aggravates AD-like pathology of APP/PS1 mice. *Brain Pathol* (in press).
 17. Gaberel T, Gakuba C, Goulay R, Martinez De Lizarrondo S, Hanouz JL, Emery E, Touze E, Vivien D, Gauberti M (2014) Impaired glymphatic perfusion after strokes revealed by contrast-enhanced MRI: a new target for fibrinolysis? *Stroke* 45:3092-3096.
 18. Luo C, Yao X, Li J, He B, Liu Q, Ren H, Liang F, Li M, Lin H, Peng J, Yuan TF, Pei Z, Su H (2016) Paravascular pathways contribute to vasculitis and neuroinflammation after subarachnoid hemorrhage independently of glymphatic control. *Cell Death Dis* 7:e2160.
 19. Sun BL, Xia ZL, Wang JR, Yuan H, Li WX, Chen YS, Yang MF, Zhang SM (2006) Effects of blockade of cerebral lymphatic drainage on regional cerebral blood flow and brain edema after subarachnoid hemorrhage. *Clin Hemorheol Microcirc* 34:227-232.
 20. Sun BL, Xie FM, Yang MF, Cao MZ, Yuan H, Wang HT, Wang JR, Jia L (2011) Blocking cerebral lymphatic drainage deteriorates cerebral oxidative injury in rats with subarachnoid hemorrhage. *Acta Neurochir Suppl (Wien)* 110:49-53.
 21. Tait MJ, Saadoun S, Bell BA, Verkman AS, Papadopoulos MC (2010) Increased brain edema in Aqp4-null mice in an experimental model of subarachnoid hemorrhage. *Neuroscience* 167:60-67.
 22. Kamp MA, Dibué M, Sommer C, Steiger HJ, Schneider T, Hänggi D (2014) Evaluation of a murine single-blood-injection SAH model. *PLoS One* 9:e114946.
 23. Garcia JH, Wagner S, Liu KF, Hu XJ (1995) Neurological deficit and extent of neuronal necrosis attributable to middle cerebral artery occlusion in rats. Statistical validation. *Stroke* 26:627-634.
 24. Huang H, Wang L, Cao M, Marshall C, Gao J, Xiao N, Hu G, Xiao M (2015) Isolation housing exacerbates Alzheimer's disease-like pathophysiology in aged APP/PS1 mice. *Int J Neuropsychopharmacol* 18:pyu116.
 25. Li X, Kong H, Wu W, Xiao M, Sun X, Hu G (2009) Aquaporin-4 maintains ependymal integrity in adult mice. *Neuroscience* 162:67-77.
 26. Xu Z, Xiao N, Chen Y, Huang H, Marshall C, Gao J, Cai Z, Wu T, Hu G, Xiao M (2015) Deletion of aquaporin-4 in APP/PS1 mice exacerbates brain A β accumulation and memory deficits. *Mol Neurodegener* 10:58.
 27. Engelhardt B, Vajkoczy P, Weller RO (2017) The movers and shapers in immune privilege of the CNS. *Nat Immunol* 18:123-131.
 28. Andreasson KI, Bachstetter AD, Colonna M, Ginhoux F, Holmes C, Lamb B, Landreth G, Lee DC, Low D, Lynch MA, Monsonego A, O'Banion MK, Pekny M, Puschmann T, Russek-Blum N, Sandusky LA, Selenica ML, Takata K, Teeling J, Town T, Van Eldik LJ (2016) Targeting innate immunity for neurodegenerative disorders of the central nervous system. *J Neurochem* 138:653-693.
 29. Verkhratsky A, Matteoli M, Parpura V, Mothet JP, Zorec R (2016) Astrocytes as secretory cells of the central nervous system: idiosyncrasies of vesicular secretion. *EMBO J* 35:239-257.
 30. Cai J, Xu D, Bai X, Pan R, Wang B, Sun S, Chen R, Sun J, Huang Y (2017) Curcumin mitigates cerebral vasospasm and early brain injury following subarachnoid hemorrhage via inhibiting cerebral inflammation. *Brain Behav* 7:e00790.
 31. German JW, Gross CE, Giclas P, Watral W, Bednar MM (1996) Systemic complement depletion inhibits experimental cerebral vasospasm. *Neurosurgery* 39:141-145.
 32. Cao X, Xu H, Feng W, Su D, Xiao M (2018) Deletion of aquaporin-4 aggravates brain pathology after blocking of the meningeal lymphatic drainage. *Brain Res Bull* 143:83-96.
 33. Yin M, Pu T, Wang L, Marshall C, Wu T, Xiao M (2018) Astroglial water channel aquaporin 4-mediated glymphatic clearance function: a determined factor for time-sensitive treatment of aerobic exercise in patients with Alzheimer's disease. *Med Hypotheses* 119:18-21.
 34. Sun BL, Wang LH, Yang T, Sun JY, Mao LL, Yang MF, Yuan H, Colvin RA, Yang XY (2018) Lymphatic drainage system of the brain: a novel target for intervention of neurological diseases. *Prog Neurobiol* 163-164:118-143.
 35. Radjavi A, Smirnov I, Derecki N, Kipnis J (2014) Dynamics of the meningeal CD4(+) T-cell repertoire are defined by the cervical lymph nodes and facilitate cognitive task performance in mice. *Mol Psychiatry* 19:531-533.
 36. Ren Z, Iliff JJ, Yang L, Yang J, Chen X, Chen MJ, Giese RN, Wang B, Shi X, Nedergaard M (2013) 'Hit & Run' model of closed-skull traumatic brain injury (TBI) reveals complex patterns of post-traumatic AQP4 dysregulation. *J Cereb Blood Flow Metab* 33:834-845.
 37. Bloch O, Auguste KI, Manley GT, Verkman AS (2006) Accelerated progression of kaolin-induced hydrocephalus in aquaporin-4-deficient mice. *J Cereb Blood Flow Metab* 26:1527-1537.
 38. Saadoun S, Bell BA, Verkman AS, Papadopoulos MC (2008) Greatly improved neurological outcome after spinal cord

- compression injury in AQP4-deficient mice. *Brain* 131:1087-1098.
39. Haj-Yasein NN, Vindedal GF, Eilert-Olsen M, Gundersen GA, Skare Ø, Laake P, Klungland A, Thorén AE, Burkhardt JM, Ottersen OP, Nagelhus EA (2011) Glial-conditional deletion of aquaporin-4 (Aqp4) reduces blood-brain water uptake and confers barrier function on perivascular astrocyte endfeet. *Proc Natl Acad Sci U S A* 108:17815-17820.
 40. Bansal R, Hao X, Liu F, Xu D, Liu J, Peterson BS (2013) The effects of changing water content, relaxation times, and tissue contrast on tissue segmentation and measures of cortical anatomy in MR images. *Magn Reson Imaging* 31:1709-1730.
 41. Neeb H, Zilles K, Shah NJ (2006) Fully-automated detection of cerebral water content changes: study of age- and gender-related H₂O patterns with quantitative MRI. *Neuroimage* 29:910-922.
 42. Timaru-Kast R, Luh C, Gotthardt P, Huang C, Schäfer MK, Engelhard K, Thal SC (2012) Influence of age on brain edema formation, secondary brain damage and inflammatory response after brain trauma in mice. *PLoS One* 7:e43829.
 43. Hladky SB, Barrand MA (2014) Mechanisms of fluid movement into, through and out of the brain: evaluation of the evidence. *Fluids Barriers CNS* 11:26.